A Low-Cost Submicrolinear Incremental Encoder Based on 3×3 Fiber-Optic Directional Coupler

H. W. Chow, Norbert C. Cheung, *Senior Member, IEEE*, and W. Jin, *Senior Member, IEEE*

***Abstract*—A high-precision displacement sensor has been developed for short-distance measurement with the interferometric method. This sensor uses a 3×3 fiber-optic directional coupler and a high-coherence laser source with 1550-nm wavelength to produce two interference patterns. A Lissajous figure is generated based on these two patterns. The change in displacement can be obtained after signal comparing and processing. Low cost and high precision are the main advantages of this sensor. Two signal-processing approaches are presented for displacement measurement.**

***Index Terms*—Coupler, displacement measurement, laser measurement applications, optical fiber interference, optical interferometry.**

I. Introduction

FIBER-OPTICS-BASED sensors are widely used for detecting kinematic and dynamic parameters such as linear displacement, angular velocity, strain, etc. Many industrial applications prefer using fiber-optics-based sensors because these sensors have many advantages over conventional electronic sensors. For example, fiber-optics-based sensors are immune to electromagnetic interference, maintenance is unnecessary since they do not include a moving part, and they have a long operating life of more than 25 years.

One popular and powerful type of fiber-optics-based sensor is the interferometer. This type of sensor is based on the interference pattern produced by the sensor itself. This variation of pattern depends on the measurement parameter. The resolution usually depends on the wavelength of the laser source, which is in the micrometer order. The interferometer is particularly suitable for high-precision measurement. For example, a nanoscale displacement measurement sensor is used in the microelectromechanical system in [1], and an add-on measurement system for a microscope using laser interferometer is described in [2]. The interferometer can also be used together with the ray-tracing method for identifying the object's position [3]. In [4], an interferometer with speckle tracking technique is used for displacement measurement on a diffusing target. In addition, a laser-diode feedback interferometer that is used for stabilizing the laser output is shown in [5].

Manuscript received June 10, 2008; revised October 24, 2008. First published April 5, 2010; current version published May 12, 2010. This work was supported by the Hong Kong Polytechnic University under Research Account RP47. The Associate Editor coordinating the review process for this paper was Dr. Juha Kostamovaara.

The authors are with the Department of Electrical Engineering, Hong Kong Polytechnic University, Kowloon, Hong Kong (e-mail: norbert.cheung@polyu.edu.hk).

Color versions of one or more of the figures in this paper are available online at http://ieeexplore.ieee.org.

Digital Object Identifier 10.1109/TIM.2009.2021622

However, the basic form of the interferometer is only able to detect the object distance instead of displacement. Recently, many engineers have developed a displacement sensor with the interferometer. References [2]–[9] show some modified interferometers used for detecting the direction and displacement. For example, the interferometer output light vector can be decomposed into two orthogonal vectors for direction detection [6]. Optical frequency modulation and digital signal processing can also be applied to the interferometer for detecting the vibrating velocity and thus calculating the displacement [7]. In [8], the automatic gain control made by an optical attenuator and a photodetector feedback is used during displacement measurement. In [9], Danati proposed a displacement sensor using a He–Ne Zeeman stabilized laser and permanent magnets. This sensor uses field backscattered from the moving surface to perform signal amplitude modulation and signal frequency modulation. The interference signals are demodulated by the electric circuit and then generate velocity and position. However, those methods usually required many extra hardware components that cause the size of the sensor to become bulky. Light beam alignment is also required since an extra optical component is required; thus, this has to increase the cost of the sensor during production.

Reference [10] shows an innovative method using an optical passive component called the 3× 3 directional coupler. It can form an interferometer that is able to produce two interference patterns with 120° phase difference. By using these two signals, displacement of the moving object can be obtained. However, the measurement range of this method is limited up to 15 μm due to its low coherence source. In addition, a high-speed processor is required to produce high resolution.

This paper proposes a new method for producing an improved interferometer. A low-cost 3×3 interferometric displacement sensor with high coherence source is designed. This method has an innovation feature of cost reduction and minimization on the number of hardware components. No extra hardware is required for optical modulation. Therefore, no extra effort on optical alignment is required. In addition, a high-coherence-length light source is used, and the measurement range could dramatically be increased. The coherence length of our light source could be used up to several tens of meters. Therefore, the measurement range could be much longer than the range obtained with the method in [10].

II. Theory

A. Fiber-Optic Interferometer With 3×3 Directional Coupler

The optical signals produced by the laser and the interferometer can be explained by using an unfolded form of

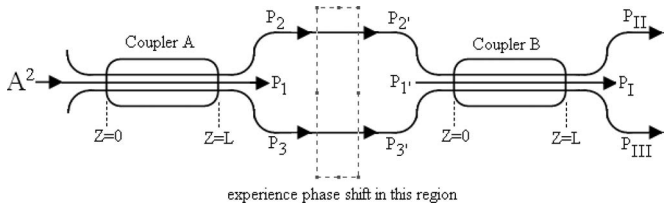

Fig. 1. Unfolded form of the interferometer with 3×3 directional coupler.

Mach–Zehnder interferometer with 3×3 directional coupler (Fig. 1). This can also be seen as an equivalent optical circuit of the displacement sensor. References [11] and [12] show that the 3×3 couplers are characterized by the coupling coefficient $K_{ij} = K_{ji}$ between the jth and ith waveguide ($i, j = 1, 2, 3$ and $i \neq j$). The complex amplitudes a_j of the three waves in the coupler are governed by the following set of linear differential equations:

$$\begin{aligned} \frac{da_1}{dz} + iK_{12}a_2 + iK_{13}a_3 &= 0 \\ \frac{da_2}{dz} + iK_{23}a_3 + iK_{21}a_1 &= 0 \\ \frac{da_3}{dz} + iK_{31}a_1 + iK_{32}a_2 &= 0 \end{aligned} \tag{1}$$

where a_j's are the complex amplitudes of the three waves in a coupler, and they are functions of z. z is the position inside the 3×3 directional coupler. In addition, $K_{12} = K_{23} = K_{31} = K$ is assumed for mathematics simplicity.

Considering Fig. 1 and the input power A^2 as the input condition of coupler A, this means that the input conditions are

$$a_1(0) = A \qquad a_2(0) = a_3(0) = 0. \tag{2}$$

For $z = L$, which is the coupling length of the coupler, (1) can be solved, and the solutions for a_j are the following:

$$\begin{aligned} |a_1(L)|^2 &= A^2 - 2\left|a_2(L)^2\right| \\ |a_2(L)|^2 = |a_3(L)|^2 &= \frac{2}{9}A^2(1 - \cos 3KL) \end{aligned} \tag{3}$$

where $|a_1(L)|^2$, $|a_2(L)|^2$, and $|a_3(L)|^2$ appear at fibers P_1, P_2, and P_3, respectively. K is the coupling coefficient. L is the coupling length of the coupler.

Two signal outputs from the coupler (P_2 and P_3) are then experienced as a phase shift ϕ and become P'_2 and P'_3, respectively. Note that ϕ resulted from the position of the moving target, and this is shown in Section II-B. Suppose $2 \cdot |a_2(L)|^2 = B^2$, where B is a constant. Then, the input condition of coupler B becomes

$$a_1(0) = 0 \quad a_2(0) = \frac{B}{\sqrt{2}}e^{i\phi} \quad a_3(0) = \frac{B}{\sqrt{2}}, \qquad B^2 \geq 0 \tag{4}$$

where ϕ is the phase difference experienced inside the interferometer. Referring to [11] and [12], the output for ports $\mathrm{P_I}$, $\mathrm{P_{II}}$, and $\mathrm{P_{III}}$ becomes

$$\begin{aligned} &|a_{\mathrm{I}}(\phi, L)|^2 \\ &\quad = \frac{2}{9}B^2(1 - \cos 3\ \mathbf{KL})(1 + \cos\phi) \\ &|a_{\mathrm{II,III}}(\phi, L)|^2 \\ &\quad = \frac{1}{18}B^2\left[(7 + 2\cos 3KL)\right. \\ &\qquad \left. - 2\cos\phi(1 - \cos 3KL)\mu 6\sin\phi\sin 3KL\right] \end{aligned} \tag{5}$$

where a_{II} takes the minus sign, and a_{III} takes the plus sign, and $|a_{\mathrm{I}}(\phi, L)|^2$, $|a_{\mathrm{II}}(\phi, L)|^2$, and $|a_{\mathrm{III}}(\phi, L)|^2$ appear at fibers $\mathrm{P_I}$, $\mathrm{P_{II}}$, and $\mathrm{P_{III}}$, respectively.

Equation (5) shows those outputs of the 3×3 interferometer ($\mathrm{P_I}$, $\mathrm{P_{II}}$, and $\mathrm{P_{III}}$) that are varying with the phase difference ϕ experienced inside the interferometer. For our case, a 3×3 coupler with 33 : 33 : 33 coupling ratio is used, and KL is supposed to be 30°.

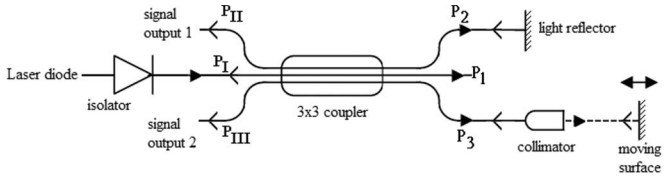

Fig. 2. Optical circuit for the displacement sensor.

B. Displacement Measurement Sensor With 3×3 Directional Coupler

Fig. 2 shows the optical component connection of the displacement measurement sensor. The laser diode generates a laser beam with input power A^2 and launches into $\mathrm{P_I}$ through the optical isolator. The function of the isolator is to prevent the reflected power from damaging and unstabilizing the laser diode. Outputs at P_1, P_2, and P_3 are expected, as shown in (3). The output signals from ports P_2 and P_3 experience reflection from the light reflector and the moving target. They also experience phase shift due to the position of the moving target. Supposing that the distance traveled from the coupler to the light reflector through P_2 and then back to the coupler is D_2, then the distance traveled from the coupler to the moving surface through P_3 and the collimator and then back to the coupler is D_3. D_2 and D_3 can be expressed as

$$\begin{aligned} D_2 &= 2L_2 \\ D_3 &= 2L_3 + 2L \end{aligned} \tag{6}$$

where L_2 is the optical length of fiber of P_2, L_3 is the optical length of fiber of P_3, and L is the optical distance between the moving surface and the collimator. The refractive index has already been taken into account.

If the wavelength of the laser is λ, then the phase difference between the reflected signals in P_2 and P_3 can be expressed as

$$\phi = (D_3 - D_2)\frac{2\pi}{\lambda} = \frac{4\pi}{\lambda}(L_3 - L_2) + \frac{4\pi L}{\lambda} \tag{7}$$

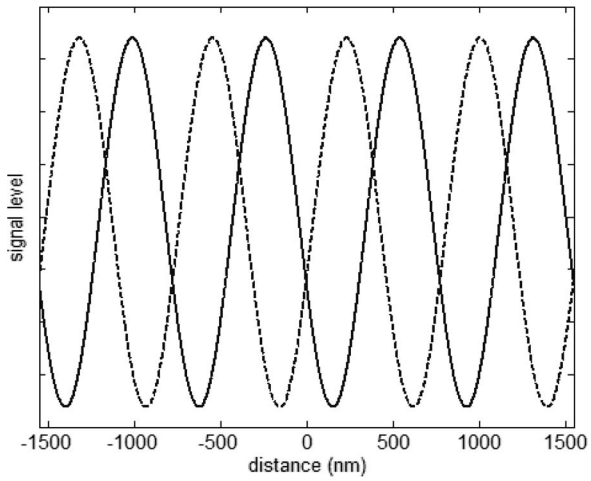

Fig. 3. Simulation result of the signal output from PII and PIII. The outputs vary with the position of the moving target.

where L_2 and L_3 are fixed, since they are the lengths of the fiber, and ϕ is then varying with L only. Light beams are recoupled into the coupler after experiencing phase shift ϕ and then undergo interference inside the coupler. It is not difficult to understand that the equations of the signal outputs of $\mathrm{P_{II}}$ and $\mathrm{P_{III}}$ are the same as in (5), with ϕ equal to (7). Graphical presentations of the signal outputs of $\mathrm{P_{II}}$ and $\mathrm{P_{III}}$ are shown in Fig. 3, where KL is set to 30°, and $L_2 \approx L_3$. According to Fig. 3, the output amplitudes are varying with the position of the moving surface. Note that the amplitudes depend on the position of the moving target, but not on time.

C. Encoding for the Signal Output From Coupler

Some problems are expected to occur in both signal outputs of the interferometer. For example, the amplitudes of the output signals will vary because the optical power is sensitive to the temperature and stress applied on the fiber. The phase difference between both optical signals is 120° (shown in Fig. 3) and not 90° (which is used in conventional encoder). A suitable encoding is required. Fig. 4 shows a flowchart of all the signal processing carried in the encoding processes.

The first processing is "offset and gain compensation." To obtain the Lissajous figure in a regular manner, the dc components of both signals have to be removed, and their amplitudes should be equal. The compensation function is achieved by detecting the upper and lower envelopes of the signals. The offset and gain compensation values (C_{off} and C_{gain}, respectively) are

$$C_{\mathrm{off}} = \frac{[ue(t) + le(t)]}{2} \tag{8}$$

$$C_{\mathrm{gain}} = \frac{2}{[ue(t) + le(t)]} \times \text{required\_amplitude} \tag{9}$$

where $ue(t)$ and $le(t)$ denote the upper and lower envelopes, respectively. Note that they are a function of time. These two compensation values adjust the signal outputs into pure ac with the same amplitude.

Suppose that the offset- and gain-compensated outputs are signal A and signal B. If they are plotted into Lissajous format, then Fig. 5 can be obtained, and the "position point" on the ellipse rotates in the clockwise and anticlockwise directions while the object is moving forward and backward, respectively.

To increase the resolution of the sensor, the second signal that processes "signal comparison" is carrying out four conditions, as shown in Fig. 5. The figure is divided into eight regions according to Table I. Assuming that the target moves at a constant speed in the forward direction, the time for traveling in each region shown in Fig. 5 is the same. Fig. 6(a) and (b) could be obtained when the target is moving. Note that Fig. 6(a) shows an analog form of the compared signals, and Fig. 6(b) shows the digital form of the compared signals. It is reminded that x and y are signal A and signal B, respectively.

It is obvious that the four digital signals have a 45° phase difference. By applying combinational logic with the truth table shown in Table II to these four signals, two square-wave signals with 90° phase shifted could be obtained. The resolution of this type of encoder is $\lambda/16$. λ is the wavelength of the laser beam.

III. Experimental Setup

To demonstrate the proposed measuring method, all the optical components were connected, as shown in Fig. 7(a) and (b). A 3×3 interferometer and a 1550-nm-high coherence laser source (new focus, external-cavity tunable diode laser, model number: 6262) controlled by a laser driver (new focus, including an external-cavity tunable diode laser controller, model number: 6200) were used. A mirror was mounted on the moving target with a movable range of 1 cm. The light reflector was replaced by a fiber reflector, as proposed by Mortimore [13]. Two p-i-n photodiode outputs were preamplified by the transimpedance amplifiers and then coupled to a 12-bit A/D converter embedded on a dSPACE DS1104 digital signal processing board for real-time measurement. An optical encoder with 50-nm resolution (Renishaw, linear optical encoder, RGH24H30D30A) was also installed for the reference displacement of the moving target, and it was connected to the dSPACE board. During the experiment, the operating temperature of the laser is controlled at 17 °C by the laser driver, and the room temperature is 22 °C.

The whole signal processing system shown in Fig. 4 was programmed into the digital signal processor (DSP) board for real-time processing. Note that the minimum sampling time of the DSP board is 50 μs, which limited the speed of the moving target since signals from the transimpedance amplifiers had to be recovered using adequate sampling points. During the experiment, the position of the moving target measured by the optical encoder and the outputs of the transimpedance amplifiers were measured at the same time.

The "offset and gain compensation" used in signal processing achieved the compensation by detecting the envelopes of the signals. However, this compensation function cannot detect envelopes when the speed of the moving target is too slow. In our experiment, the "offset and gain compensation" function was terminated when the speed of the moving target was slower

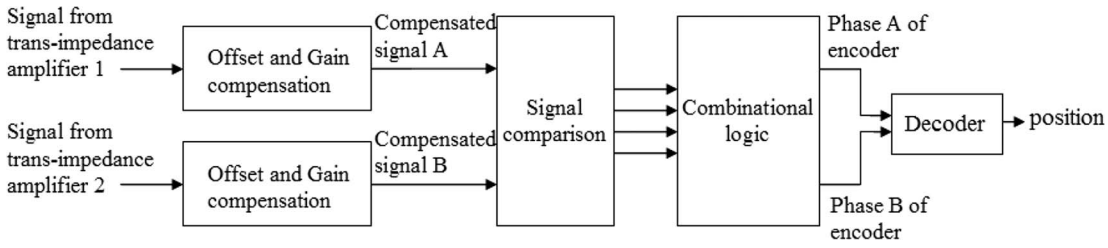

Fig. 4. Flowchart of signal processing.

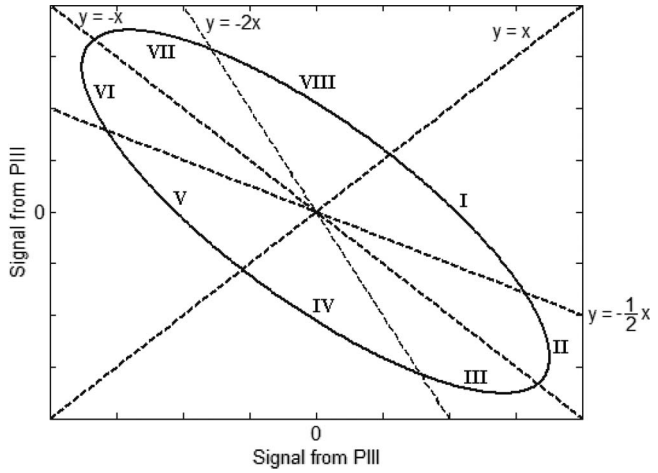

Fig. 5. Lissajous figure with signal A and signal B for x- and y-axes. Note that this is obtained from simulation.

TABLE I
CONDITION FOR REGION

y−x	y+(1/2)x	y+x	y+2x	Region
−ve	+ve	+ve	+ve	I
−ve	−ve	+ve	+ve	II
−ve	−ve	−ve	+ve	III
−ve	−ve	−ve	−ve	IV
+ve	−ve	−ve	−ve	V
+ve	+ve	−ve	−ve	VI
+ve	+ve	+ve	−ve	VII
+ve	+ve	+ve	+ve	VIII

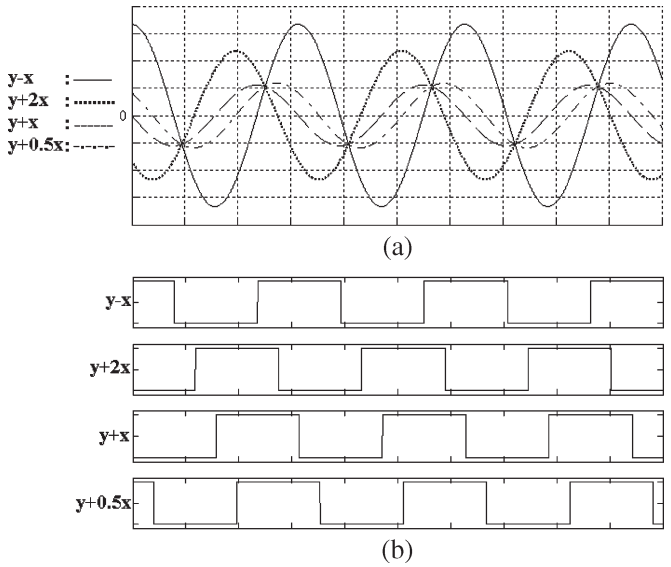

Fig. 6. Output from process "signal comparison" from simulation (x-axis is the time in seconds).

TABLE II
REDEFINED OUTPUT SIGNALS

	+ve	−ve
Phase A	I, II, V, VI	III, IV, VII, VIII
Phase B	II, III, VI, VII	I, IV, V, VIII

than 0.4 mm/s, and the compensation value will set to values just before termination.

The lower limit of the speed is due to the compensator. However, the upper limit is due to the sampling rate of the dSPACE board. The maximum speed of the target is

$$V_{\max} = \frac{\lambda/2}{(2 \times n_{\text{condition}} \times t_{\text{sampling}})} \tag{10}$$

where λ is the operating wavelength of the laser, $n_{\text{condition}}$ is the number of conditions used, and t_{sampling} is used in the signal processor. Note that $2 \times n_{\text{condition}}$ is the minimum number of sampling points to recover the signal.

There are three different situations that were investigated: 1) the target moves in the forward direction; 2) the target moves in the backward direction; and 3) the target changes its moving direction. In each situation, phase A and phase B were produced by the two different methods. The first method used the conditions and logic mentioned in Tables I and II. The other method used the digital form of the signals "$y - x$" and "$y + x$" shown in Fig. 6(b) to act as phase A and phase B. In total, six results could be obtained for the three different situations. The resolution of the first approach is equal to $\lambda/16 = (1550/16) = 96.8$ nm. The square wave generated by the first approach is twice as dense as the second approach; therefore, the resolution is $\lambda/8 = (1550/8) = 193.75$ nm.

Note that $V_{\max}$ is calculated based on (10), and therefore, the $V_{\max}$ of the 97-nm-resolution case is 3.875 mm/s when $n_{\text{condition}}$ is 4, and the $V_{\max}$ of the 194-nm-resolution case is 1.9375 mm/s when $n_{\text{condition}}$ is 2.

For each situation, six sets of data were collected: 1) signals from two transimpedance amplifiers; 2) two square waves (phase A and phase B) with 90° phase shift produced by signal processing; 3) displacement recorded by the optical encoder; 4) displacement converted from this two square waves by the decoder; 5) error between the displacement measured by the proposed methods and the optical encoder; and 6) the velocity of the moving target was recorded. Note that the velocity of the moving target recorded in 6) was calculated by optical encoder measurement, and all the data were collected from a

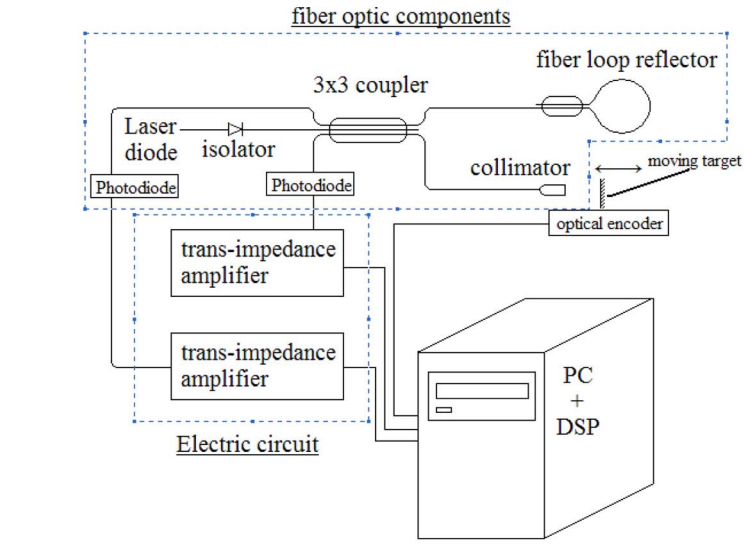

(a)

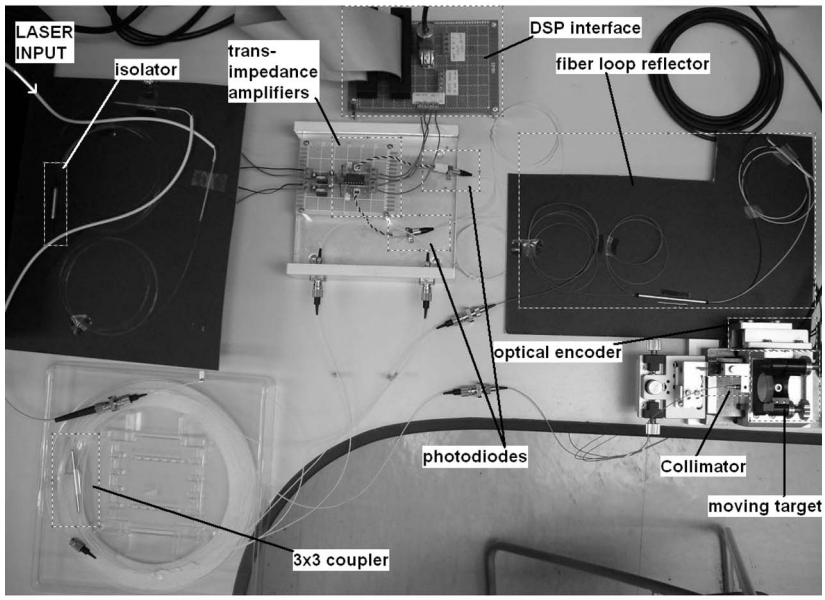

(b)

Fig. 7. (a) Diagram for setup of the interferometer displacement sensor. (b) Actual object for setup of the interferometer displacement sensor.

real-time process. Figs. 8–13 show those plots for situations 1, 2, and 3.

IV. Performance and Discussion

A. Maximum Velocity of Moving Object

Fig. 10 demonstrates the target moving at different velocities and reversing its direction with the 194-nm-resolution measurement approach, and the error-time graph in Fig. 10(e) is showing a sudden increase when the speed of the target is larger than 2.5 mm/s. A similar situation occurs in Fig. 13, which is measured by using the 97-nm-resolution approach. A sudden increase in the error curve [Fig. 13(e)] occurs when the speed of the target is larger than 1.5 mm/s.

The measured maximum speeds are different from the calculated values. It is because the number of sampling points in (10) is not adequate for recovering the signal. Therefore, (10) should be modified. The new maximum speed equation is

$$V_{\max} = \frac{1}{1.5} \frac{\lambda/2}{(2 \times n_{\text{condition}} \times t_{\text{sampling}})}. \tag{11}$$

Note that the 1.5 value in (11) is the compensation factor for the minimum number of sampling points.

The reason for the sudden increase in the error curve is due to the speed of the moving target. When the speed is larger than the critical value (2.5 mm/s for 194-nm resolution and 1.2917 mm/s for 97-nm resolution), the number of sampling points is not enough for reconstructing the waveforms. It can be observed in Figs. 10(a) and 13(a).

To conclude, the maximum speed of the moving target is limited by the sampling rate of the analog-to-digital converter (ADC). The ADC used in this project is for a general purpose,

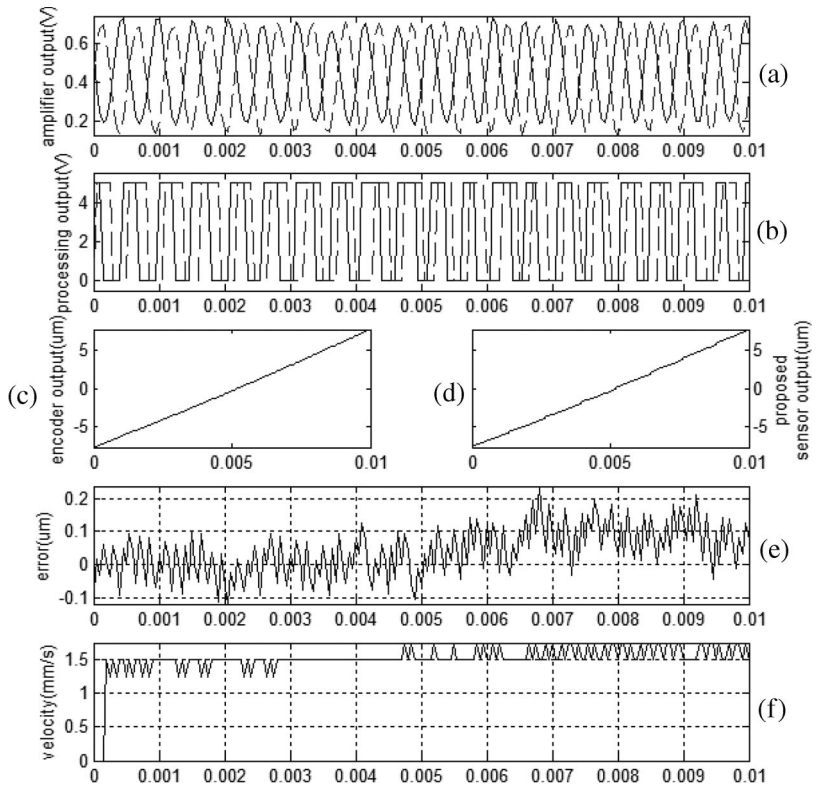

Fig. 8. Data capture for situation 1 with a resolution of 194 nm, and the x-axis is the time in seconds (the target moves in the forward direction). (a) Signals collected from two transimpedance amplifiers. (b) Phase A and phase B from signal processing. (c) Displacement measurement from the optical encoder. (d) Displacement measurement using the proposed sensor. (e) Difference between the measurement of the optical encoder and the proposed sensor. (f) Velocity of the moving target.

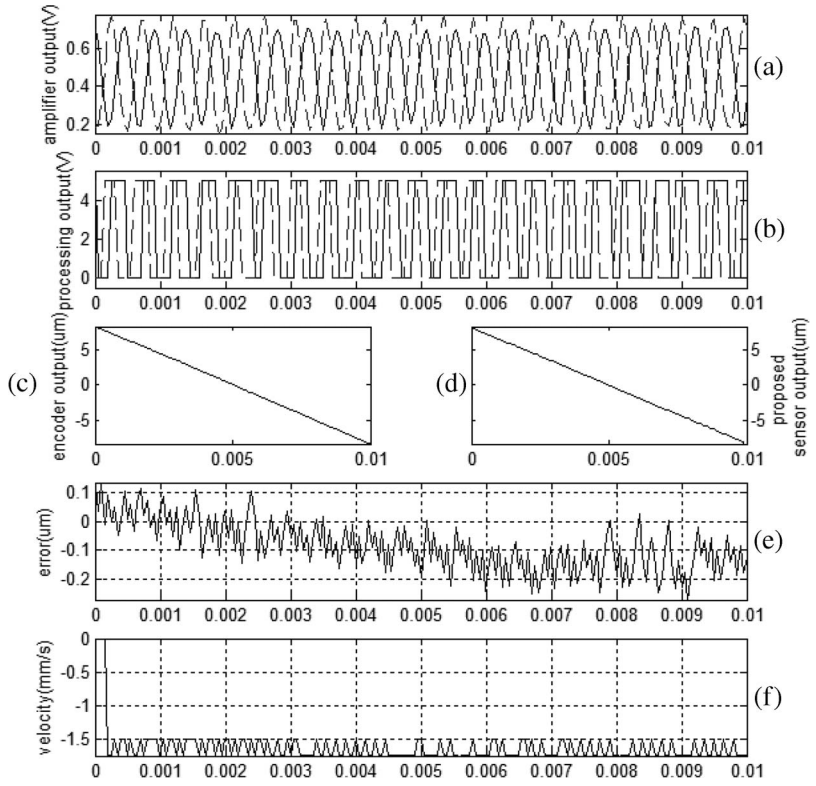

Fig. 9. Data capture for situation 2 with a resolution of 194 nm, and the x-axis is the time in seconds (the target moves in the backward direction). (a) Signals collected from two transimpedance amplifiers. (b) Phase A and phase B from signal processing. (c) Displacement measurement from the optical encoder. (d) Displacement measurement using the proposed sensor. (e) Difference between the measurement of the optical encoder and the proposed sensor. (f) Velocity of the moving target.

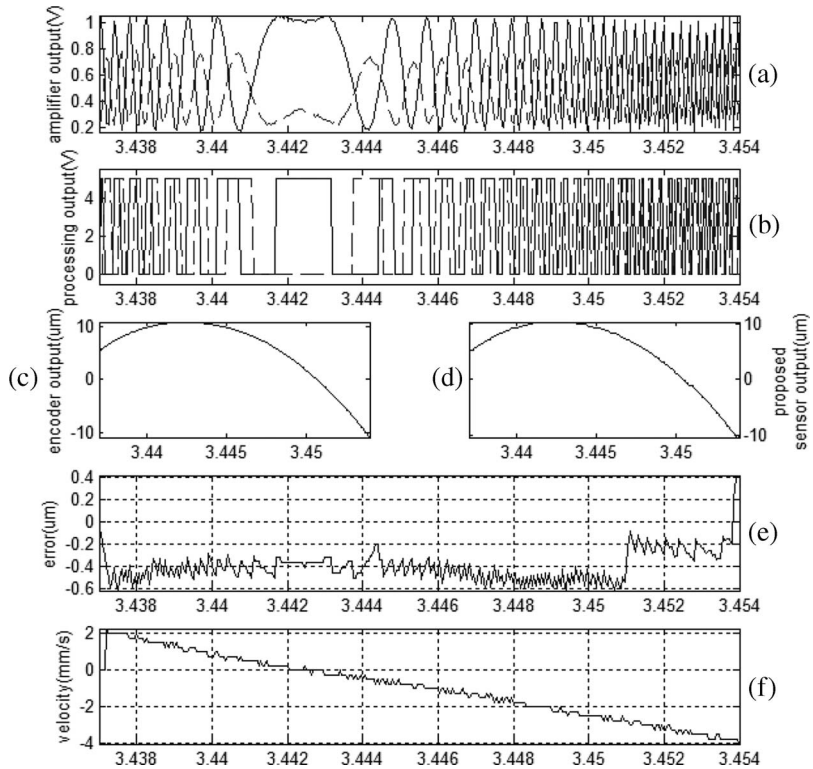

Fig. 10. Data capture for situation 3 with a resolution of 194 nm, and the x-axis is the time in seconds (the target changes the moving direction). (a) Signals collected from two transimpedance amplifiers. (b) Phase A and phase B from signal processing. (c) Displacement measurement from the optical encoder. (d) Displacement measurement using the proposed sensor. (e) Difference between the measurement of the optical encoder and the proposed sensor. (f) Velocity of the moving target.

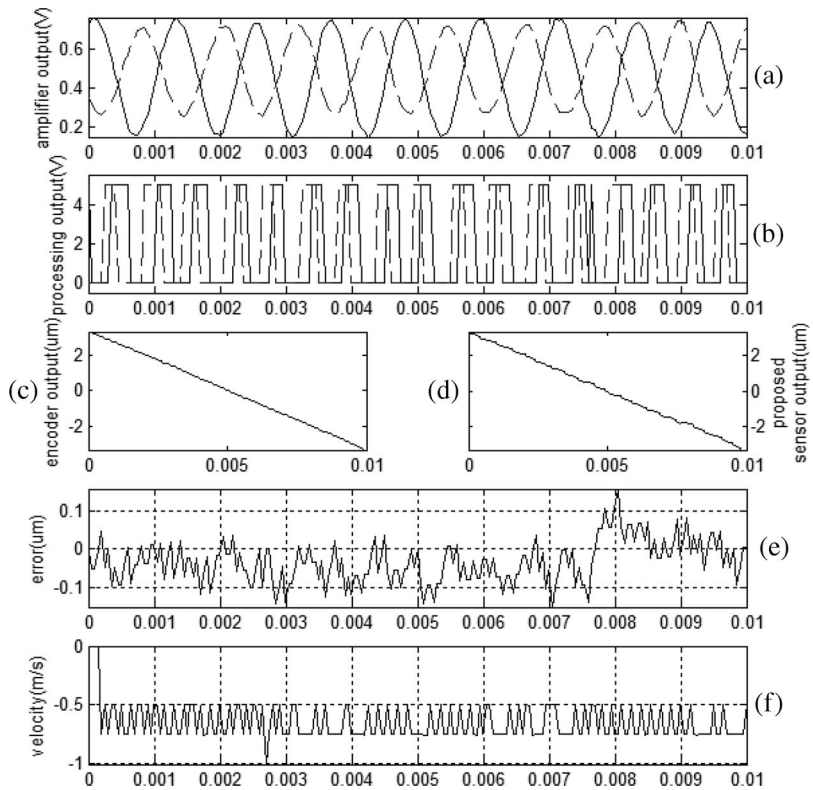

Fig. 11. Data capture for situation 1 with a resolution of 97 nm, and the x-axis is the time in seconds (the target moves in the forward direction). (a) Signals collected from two transimpedance amplifiers. (b) Phase A and phase B from signal processing. (c) Displacement measurement from the optical encoder. (d) Displacement measurement using the proposed sensor. (e) Difference between the measurement of the optical encoder and the proposed sensor. (f) Velocity of the moving target.

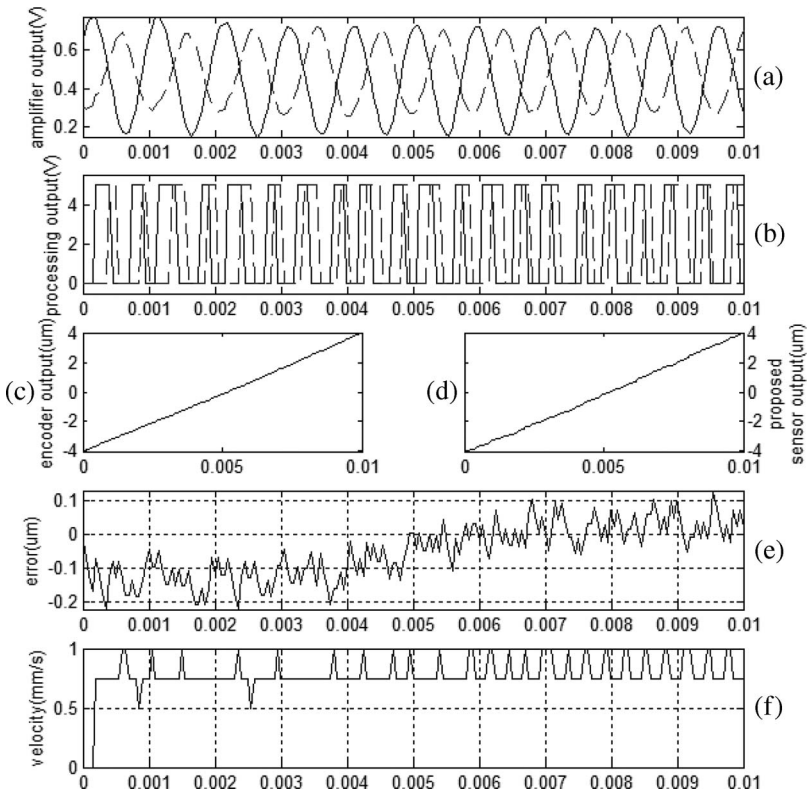

Fig. 12. Data capture for situation 2 with a resolution of 97 nm, and the x-axis is the time in seconds (the target moves in the backward direction). (a) Signals collected from two transimpedance amplifiers. (b) Phase A and phase B from signal processing. (c) Displacement measurement from the optical encoder. (d) Displacement measurement using the proposed sensor. (e) Difference between the measurement of the optical encoder and the proposed sensor. (f) Velocity of the moving target.

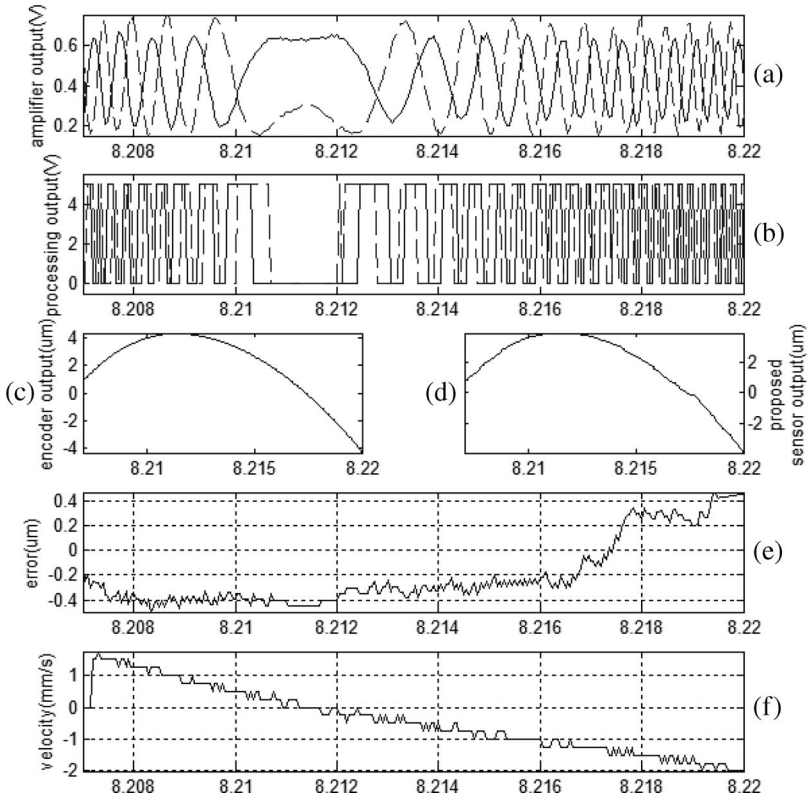

Fig. 13. Data capture for situation 3 with a resolution of 97 nm, and the x-axis is the time in seconds (the target moves in the backward direction). (a) Signals collected from two transimpedance amplifiers. (b) Phase A and phase B from signal processing. (c) Displacement measurement from the optical encoder. (d) Displacement measurement using the proposed sensor. (e) Difference between the measurement of the optical encoder and the proposed sensor. (f) Velocity of the moving target.

and hence, the maximum speed of this sensing system seems to be too slow for industrial applications. This maximum speed could be improved by using a powerful ADC with a higher sampling rate.

B. Error of the Sensing System

The accuracy of the sensor could be evaluated by assuming that the target moves at a constant speed. Figs. 8 and 9 show that the maximum error is ± 150 nm for the 194-nm-resolution case. Figs. 11 and 12 show that the maximum error is ± 101.5 nm for the 97-nm-resolution case. On Figs. 8(e), 9(e), 10(e), 11(e), 12(e), and13(e), some special phenomena could be found: 1) the error curve is gradually increasing or decreasing; and 2) some sudden step up in the error curve.

The main reason for the first phenomenon is because the output power and the emitted wavelength of the laser source are varying with the tiny temperature variation. Although the laser is controlled by the laser driver and under temperature and wavelength control, a small temperature variation causes the laser driver to retune the laser wavelength to 1550 nm. However, a few seconds are required to settle the wavelength. The wavelength will oscillate within ± 0.5 nm. In the decoder, the displacement calculation is based on the resolution of the sensor, which is $\lambda/8$ or $\lambda/16$. The preset wavelength of the laser is assumed equal to the fixed value of 1550 nm in the DSP. A small variation in temperature will cause the wavelength drift to slightly be higher or lower than 1550 nm, and therefore, the trend of the error value is increasing and decreasing during the measurement process.

The second problem, i.e., the sudden "jump" in the error curve, is caused by noise in signal A and signal B collected from the transimpedance amplifiers. For example, during 0.0075–0.008 s, the solid line in Figs. 11(a) was affected by noise, and hence, the square wave in Figs. 11(b) produced some sharp "spikes." These "spikes" cause the encoder to accumulate the error and cause a "jump" in the error curve.

C. Stability

The measurements for a stationary target position over a period of 9 s for both cases (194- and 97-nm resolutions) were performed, and the results are shown in Figs. 14 and 15. The maximum deviation is 1 resolution of the sensor, and this could be verified from Figs. 14(b) and 15(b). Those deviations result from the noise in signal A and signal B and the external vibrations of the moving object. The signals that suffered from noise are shown in Figs. 14(a) and 15(a). It is observed that signal A and signal B consist of high- and low-frequency components. The high-frequency component resulted from the noise in the electrical circuit, whereas the low-frequency component resulted from the external vibration and an unstable temperature. Note that temperature instability will cause laser diode power fluctuation and wavelength shift.

The external vibration caused the position point to oscillate inside the Lissajous figure, although the target is stationary. When it oscillated across the region boundary, as shown in Fig. 5, a deviation in position will appear since the rising and falling edges in phase A and phase B are generated. The number of deviations for the 97-nm-resolution approach is more than the 194-nm-resolution approach since the latter has more conditions and region. Note that the measuring period (9 s in this project) is limited by the memory in the DSP.

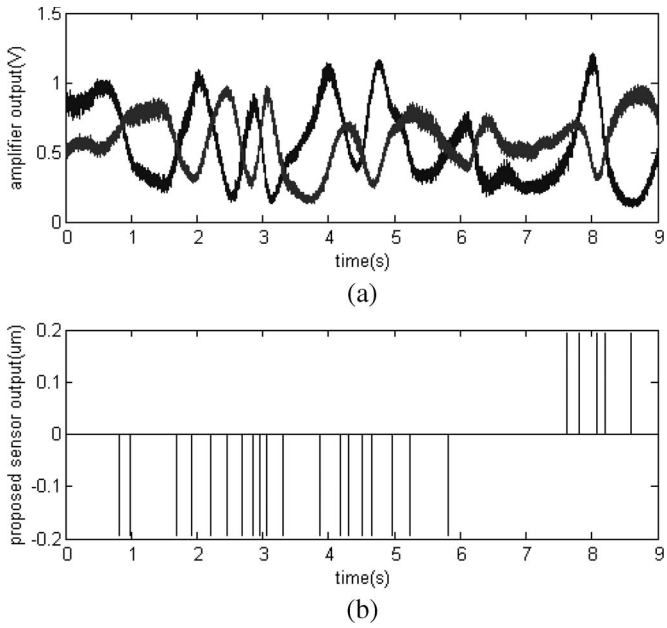

Fig. 14. Proposed measurement sensor with a 194-nm reading for a stationary target over a period of 9 s. (a) Signal collected from transimpedance amplifiers. (b) Displacement measured by the proposed method.

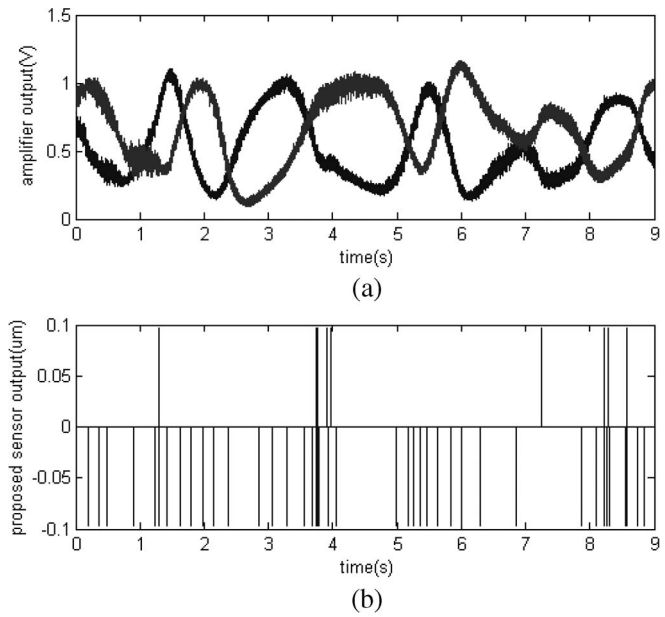

Fig. 15. Proposed measurement sensor with a 97-nm reading for a stationary target over a period of 9 s. (a) Signal collected from transimpedance amplifiers. (b) Displacement measured by the proposed method.

D. Cost Reduction

Compared with other types of interferometer, our design is more suitable for industrial application. The most important

reason is cost reduction in our design. Other sensors used some components to generate the direction information. For example, in [6], a coupler, a retarding film, and a polarizing beam splitter are used for decomposing the laser beam into two orthogonal vectors to collect displacement and direction information. In [7], the sensor includes a piezoelectric element and two lasers, which are the external-cavity tunable laser and the Zeeman laser for optical-frequency modulation to achieve displacement measurement. In [9], permanent magnets with moderate transverse field are installed and applied to the plasma tube to modulate the laser beam. However, in this paper, the displacement sensor is only using one component, i.e., a 3×3 coupler, to generate displacement of the moving object, which greatly reduces the cost. In addition, this design could minimize the number of components, reduce the difficulty during installation, reduce the number of light beam alignment, and shorten the installation time. The overall installation cost will also be reduced.

V. Conclusion

A high-precision displacement sensor with interferometric method, together with a high-coherence-length laser, is described and experimentally verified. The measurement is based on the conversion from outputs of the 3×3 coupler into two phase A and phase B square waves. The resolution of the sensor could be up to 97 and 194 nm. The maximum speed is low for high-resolution sensing, but the error is relatively low for a high-resolution output. The most expensive component in this sensing system is the external cavity tunable laser source. However, it could be replaced by a distributed feedback laser, and the tradeoff is shorter coherence length and shorter measurable range. In addition, the precision of this sensing system could further be improved by a short-wavelength laser.

The proposed method is particularly suitable for high-precision differential displacement measurement, such as the sensor of the continuous mechanical alignment in machines.

References

[1] C. W. Lee, X. M. Zhang, S. C. Tjin, and A. Q. Liu, "Nano-scale displacement measurement of MEMS device using fiber optic interferometry," *J. Inst. Eng.—Singapore*, vol. 44, no. 5, pp. 1–8, 2004.

[2] V. Augutis, D. Gailius, and P. Kuzas, "Low cost microscope add-on system for subpixel resolution displacement measurement," in *Proc. IMTC*, May 2007, pp. 1–4.

[3] A. Michalski and D. Sawicki, "The new approach to an optical noncontact method for small displacement measurements," *IEEE Instrum. Meas. Mag.*, vol. 7, no. 3, pp. 76–82, Sep. 2004.

[4] M. Norgia, S. Donati, and D. D'Alessandora, "Interferometric measurements of displacement on a diffusing target by a speckle tracking technique," *IEEE J. Quantum Electron.*, vol. 37, no. 6, pp. 800–806, Jun. 2001.

[5] S. Donati, L. Falzoni, and S. Merlo, "A PC-interfaced, compact laserdiode feedback interferometer for displacement measurements," *IEEE Trans. Instrum. Meas.*, vol. 45, no. 6, pp. 942–947, Dec. 1996.

[6] H. C. Seat, S. Pullteap, and T. Bosch, "An extrinsic fiber optic interferometer with possible signal fading compensation for vibrometric application," in *Proc. IEEE IMTC*, May 2005, pp. 2236–2241.

[7] Y. Shinoda, M. Itoh, and T. Higo, "Real-time computation of distance and displacement by software instruments using optical frequency modulation," in *Proc. SICE*, Aug. 2002, pp. 82–83.

[8] M. Norgia and S. Donati, "A displacement-measuring instrument utilizing self-mixing interferometry," *IEEE Trans. Instrum. Meas.*, vol. 52, no. 6, pp. 1765–1770, Dec. 2003.

[9] S. Danati, "Laser interferometry by induced modulation of the cavity field," *J. Appl. Phys.*, vol. 49, no. 2, pp. 495–497, Feb. 1978.

[10] M. C. Tomic, "Low-coherence interferometric method for measurement of displacement based on a 3×3 fiber-optic directional coupler," *J. Opt. A, Pure Appl. Opt.*, vol. 4, no. 6, pp. S381–S386, Nov. 2002.

[11] S. K. Sheem, "Fiber-optic gyroscope with (3×3) directional coupler," *Appl. Phys. Lett.*, vol. 37, no. 10, pp. 869–871, Nov. 1980.

[12] S. K. Sheem, "Optical fiber interferometers with 3×3 directional couplers: Analysis," *J. Appl. Phys.*, vol. 52, no. 6, pp. 3865–3872, Jun. 1981.

[13] D. B. Mortimore, "Fiber loop reflectors," *J. Lightwave Technol.*, vol. 6, no. 7, pp. 1217–1224, Jul. 1988.

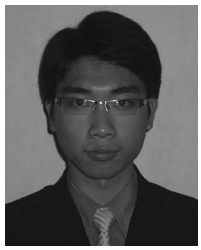

H. W. Chow was born in Hong Kong, in 1985. He received the B.Eng. degree in electrical engineering from the Hong Kong Polytechnic University, Kowloon, Hong Kong, in December 2007.

Since 2007, he has been with the Power Electronic Laboratory, Hong Kong Polytechnic University, where he is working on low-cost submicrodisplacement sensor and high-precision control.

Norbert C. Cheung (SM'05) received the B.Sc. degree from the University of London, London, U.K., in 1981, the M.Sc. degree from the University of Hong Kong, Hong Kong, in 1987, and the Ph.D. degree from the University of New South Wales, Sydney, Australia, in 1996.

He is currently an Assistant Professor with the Department of Electrical Engineering, Hong Kong Polytechnic University, Kowloon, Hong Kong. He has published more than 30 journal papers and more than 70 conference papers. He has also obtained three patent inventions. His research interests are mechatronics, instrumentation, control, industrial electronics, motors, and actuators.

W. Jin (SM'99) received the B.Eng. and M.Sc. degrees from the Beijing University of Aeronautics and Astronautics, Beijing, China, in 1984 and 1987, respectively, and the Ph.D. degree in fiber optics from the University of Strathclyde, Glasgow, U.K., in 1991.

From 1991 to 1995, he was a Postdoctoral Research Fellow with the University of Strathclyde. In 1996, he joined the Department of Electrical Engineering, Hong Kong Polytechnic University, Kowloon, Hong Kong, as an Assistant Professor, where he became an Associate Professor in 1998 and a Professor in 2003.

Dr. Jin is a member of The International Society for Optical Engineers and the Optical Society of America, and the Vice-Chairman of the Fiber and Integrated Society of China. He has served as a Technical Program Committee Member/Session Chair of over 20 international and national conferences. He also served as an assessment panel member of the National Science Foundation of China.